

VLT MUSE observations of the bubble nebula around NGC 1313 X-2 and evidence for additional photoionization

CHANGXING ZHOU,¹ FUYAN BIAN,² HUA FENG,^{3,1} AND JIAHUI HUANG¹

¹*Department of Engineering Physics, Tsinghua University, Beijing 100084, China*

²*European Southern Observatory, Alonso de Córdova 3107, Casilla 19001, Vitacura, Santiago 19, Chile*

³*Department of Astronomy, Tsinghua University, Beijing 100084, China*

ABSTRACT

The bubble nebula surrounding NGC 1313 X-2 is believed to be powered by high velocity winds from the central ultraluminous X-ray source (ULX) as a result of supercritical accretion. With the Multi-Unit Spectroscopic Explorer (MUSE) observation of the nebula, we find enhanced [O III] emission at locations spatially coincident with clusters of stars and the central X-ray source, suggesting that photoionization in addition to shock-ionization plays an important role in powering the nebula. The X-ray luminosity of the ULX and the number of massive stars in the nebula region can account for the required ionizing luminosity derived with *MAPPINGS V*, which also confirms that pure shocks cannot explain the observed emission line ratios.

Keywords: Ultraluminous x-ray sources (2164), Emission nebulae (461), Superbubbles (1656), Accretion (14)

1. INTRODUCTION

Ultraluminous X-ray sources (ULXs) are extremely accreting compact objects, and occupy the high end of the luminosity function of high mass X-ray binaries (Mineo et al. 2012). They display X-ray luminosities exceeding the Eddington limit of a typical stellar mass black hole, with spectral and timing behaviors distinct from Galactic X-ray binaries (for a review see Kaaret et al. 2017). Identification of neutron stars in ULXs (Bachetti et al. 2014; Fürst et al. 2016; Israel et al. 2017a,b; Carpano et al. 2018; Sathyaprakash et al. 2019; Rodríguez Castillo et al. 2020) and their ordinary spectral properties (Pintore et al. 2017; Walton et al. 2018) suggest that supercritical accretion occurs in the majority of these systems.

Due to the presence of strong radiation pressure, winds are expected to launch under supercritical accretion (Shakura & Sunyaev 1973; Meier 1982; Lipunova 1999; King & Pounds 2003; Poutanen et al. 2007; Shen et al. 2016). This is also predicted by numerical simulations (Ohsuga & Mineshige 2011; Jiang et al. 2014; Hashizume et al. 2015; Sądowski & Narayan 2016; Takahashi et al. 2016; Abarca et al. 2018; Kitaki et al. 2018, 2021), which all reveal that there is a central funnel where ultra-fast winds ($0.1\text{--}0.4 c$) are launched. Observationally, the wind is evidenced with the detection of high velocity absorption features in the X-ray spectra of ULXs (Pinto et al. 2016, 2017, 2021; Walton et al. 2016; Kosec et al. 2018).

Interaction of the wind with the interstellar medium (ISM) may produce shock-ionized bubble nebulae, which have been found around some ULXs (Pakull & Mirioni 2002, 2003; Ramsey et al. 2006; Abolmasov et al. 2007; Abolmasov 2008; Russell et al. 2011; Soria et al. 2021). These bubbles have a size of some 100 pc, expanding at a velocity of about 100 km s^{-1} . Based on the emission line luminosity, bubble size, and expansion velocity, the mechanical power of the wind or jet that drives the bubble is estimated to be about $10^{39}\text{--}10^{40} \text{ erg s}^{-1}$, suggesting that the accretion is supercritical (Pakull & Mirioni 2003; Abolmasov et al. 2007), in agreement with the detection of diffuse X-ray emission in one of them (Belfiore et al. 2020).

NGC 1313 X-2 is a prototype ULX among the first discovered (Colbert et al. 1995). A bubble nebula is found to be coincident with the X-ray source position and has been extensively studied (Pakull & Mirioni 2002, 2003; Zampieri et al. 2004; Mucciarelli et al. 2005; Pakull et al. 2006; Ramsey et al. 2006; Ripamonti et al. 2011). The nebula is elongated with a geometry of $590 \text{ pc} \times 410 \text{ pc}$ ($26'' \times 18''$). The presence of strong [S II] and [O I] emission lines and the supersonic expansion suggests that the nebula is shock-ionized (Pakull & Mirioni 2002, 2003), while the most likely powering source is the wind/jet from the central ULX (Pakull & Grisé 2008) with a mechanical power estimated to be about $1.5 \times 10^{39} \text{ erg s}^{-1}$ (Pakull & Mirioni 2002).

In this paper, we present a spatially resolved spectroscopic study of the bubble nebula around NGC 1313 X-2 using the MUSE instrument (Bacon et al. 2010) on the Very Large Telescope (VLT). The observations are described in § 2, the data analysis and results are presented in § 3, and the physical nature is discussed in § 4. We assume a distance of 4.6 Mpc

to NGC 1313 based on Cepheids measurements (Qing et al. 2015).

2. OBSERVATIONS

The VLT/MUSE observations of NGC1313 X-2 were performed on the nights of 2019 October 16 and November 12 (UT). The seeing during the observations was from $0''.8$ to $1''.0$, and sky transparency conditions were clear on 2019 October 16 and partially cloudy on 2019 November 12. The MUSE WFM-NOAO-E mode was used to cover the wavelength between 4600\AA and 9350\AA . The observations include four 1400-second exposures: two of them with a position angle of 0° and the rest two with an angle of 90° .

The data were reduced by the EsoRex pipeline version 3.13.2 (Weilbacher et al. 2020). We used the *muse_scibasic* recipe to correct bias frames, lamp flats, arc lamps, twilight flats, geometry, and illumination exposures for individual exposures. Then the *muse_scipost* recipe was used for telluric and flux calibrations with the standard star taken in the same night. At last the individual exposures were aligned using the *muse_exp_align* recipe and combined to generate the final datacube using the *muse_exp_combine* recipe. The field of view of the final datacube is $1' \times 1'$ and the spaxel scale is $0''.2 \times 0''.2$.

3. DATA ANALYSIS AND RESULTS

Figure 1 shows the nebula images in the $H\alpha$ band, one with line plus continuum emission and the other with line emission only. A bright object appears near the west end of the nebula, and is identified to be a foreground M1 dwarf at a distance of 750 pc (Gaia Collaboration et al. 2021) along the line of sight of the nebula (also see Ramsey et al. 2006).

We find that the nebula spectra are contaminated by unresolved stellar emission in the host galaxy projected on the nebula region (see the Hubble images in Grisé et al. 2008). The stellar emission contributes a continuum component with absorption lines, while the nebula spectrum mainly consists of emission lines. In order to remove the stellar contamination, we extract a template spectrum from a background region defined in Figure 1. For the nebula, we are only interested in the emission line properties in two bands, a blue band that contains $H\beta$ and $[\text{O III}]$, and a red band with $[\text{O I}]$, $H\alpha$, $[\text{N II}]$, and $[\text{S II}]$. We extracted the nebula spectrum from an elliptical region defined in Figure 1, and fit it with the template in the two bands, respectively, at wavelengths excluding emission lines. In the fitting, we employ a scale factor and a shift on the flux onto the template spectrum. Then the best-fit stellar template is removed from the nebula spectrum. The blue and red bands are not fitted jointly because different scales are needed. We have to assume that the stellar contamination is insensitive to the sky position, because the statistics from a small number of pixels does not allow us to perform the template fitting. The spectrum extracted from a single pixel after subtracting the stellar template exhibits fluctuations consistent with the statistical error, justifying the validity of the technique. The final spectra in the blue and red bands are shown in Figure 2.

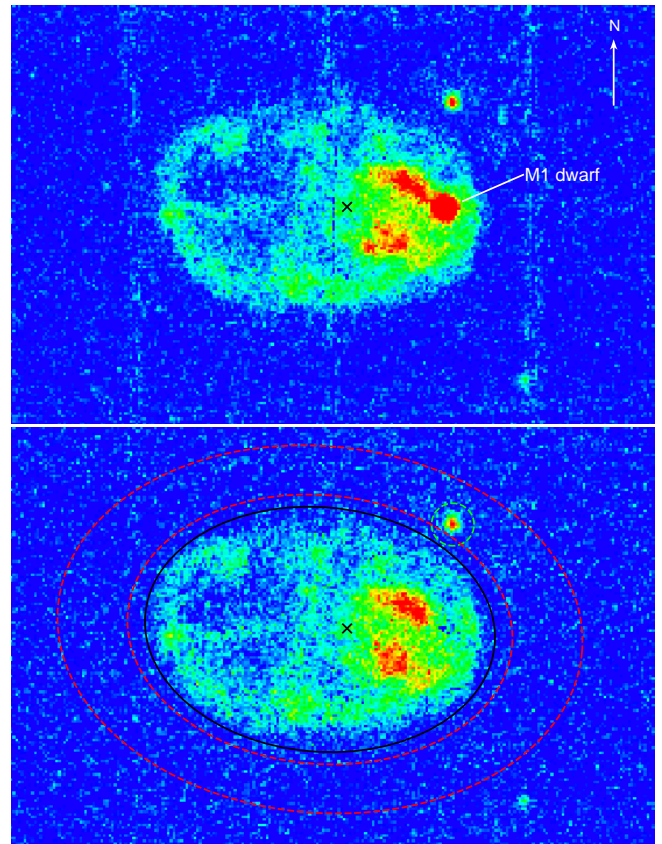


Figure 1. MUSE $H\alpha$ ($\pm 5\text{\AA}$ around the line centroid) images around NGC 1313 X-2 with (top) and without (bottom) the continuum emission. The cross marks the X-ray position of NGC 1313 X-2 (Liu et al. 2007). A foreground M1 dwarf appears along the line of sight of the nebula and is visible only with the continuum emission. The black ellipse defines the nebula region and the red dashed lines excluding a green dashed circle encircle the background region. The arrow points north and has a length of $5''$ (112 pc).

Each emission line is fitted locally with a Gaussian to a continuum subtracted spectrum. The continuum is determined with a linear function from nearby wavelengths free of the emission component. The Balmer lines are fitted independently. Either the $[\text{O III}] \lambda\lambda 4959, 5007$ or $[\text{S II}] \lambda\lambda 6716, 6731$ doublet are fitted jointly, imposing the same velocity and width; for $[\text{O III}] \lambda\lambda 4959, 5007$, we further constrain the flux ratio to be 2.98 (Storey & Zeippen 2000), which is in good agreement with the ratio derived from independent measurements. The line flux, velocity relative to the host galaxy ($z = 0.001568$ or $v = 470 \text{ km s}^{-1}$; Koribalski et al. 2004), and the full-width-half-maximum (FWHM) velocity dispersion corrected for instrument line broadening¹ are derived for bright lines and listed in Table 1 for the whole

¹ Available in Section 3.2 of the MUSE user manual, see https://www.eso.org/sci/facilities/paranal/instruments/muse/doc/ESO-261650_MUSE_User_Manual.pdf. The lines seen in nearby H II regions are found to have widths consistent with the instrument line broadenings.

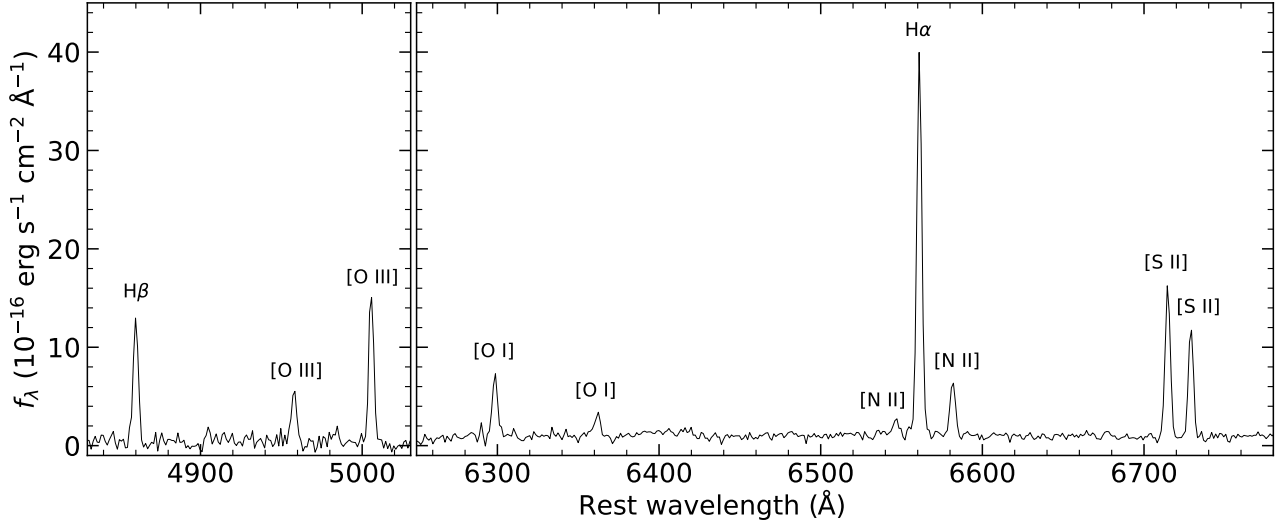


Figure 2. The MUSE spectra in the blue (left) and red (right) bands of the NGC 1313 X-2 nebula.

Table 1. The emission line flux, velocity, and velocity dispersion for the whole nebula.

| line | f (10^{-16} erg cm^{-2} s^{-1}) | v (km s^{-1}) | FWHM (km s^{-1}) | FWHM _{inst} (km s^{-1}) |
|------------------------|--|-------------------------------|--------------------------------|--|
| H β | 62.0 ± 2.9 | -87.7 ± 3.2 | 126 ± 13 | 177 ± 6 |
| [O III] λ 4959 | 26.4 ± 1.1 | -72.8 ± 2.9 | 129 ± 11 | 173 ± 6 |
| [O III] λ 5007 | 78.7 ± 3.3 | -72.8 ± 2.9 | 129 ± 11 | 171 ± 6 |
| [O I] λ 6300 | 32.8 ± 1.0 | -87.4 ± 1.6 | 121 ± 6 | 126 ± 4 |
| [O I] λ 6364 | 11.4 ± 2.2 | -88 ± 11 | 128 ± 37 | 124 ± 4 |
| [N II] λ 6548 | 8.9 ± 1.5 | -72 ± 8 | 117 ± 33 | 119 ± 4 |
| H α | 191.5 ± 2.1 | -83.7 ± 0.6 | 110 ± 2 | 119 ± 4 |
| [N II] λ 6583 | 29.4 ± 0.7 | -80.8 ± 1.3 | 127 ± 4 | 119 ± 4 |
| [S II] λ 6716 | 76.6 ± 1.6 | -80.3 ± 1.0 | 110 ± 3 | 116 ± 4 |
| [S II] λ 6731 | 55.0 ± 1.3 | -80.3 ± 1.0 | 110 ± 3 | 115 ± 4 |

NOTE— v is the relative velocity with respect to the host galaxy. FWHM has been corrected for instrument line broadening (FWHM_{inst}).

nebula. The line fluxes derived from the observation on October 16 are systematically higher than those on November 12 because of different sky conditions, and have been corrected as in the clear sky condition.

The average radial velocity of the whole nebula is around -80 km s^{-1} (negative means a blue shift) with respect to the bulk velocity of 470 km s^{-1} as mentioned above. They are consistent with the line velocities measured from three nearby, possibly H II regions. For example, one of them marked by a dashed green circle in Figure 1 has a velocity of $-81 \pm 2 \text{ km s}^{-1}$ measured with H α or $-80 \pm 2 \text{ km s}^{-1}$ with [S II]. Thus, we adopt -80 km s^{-1} as the systematic velocity. This confirms the conclusion in Pakull & Mirioni (2002) that the bubble nebula is indeed associated with the host galaxy.

To investigate the spatial distribution of the line properties, we produce the flux, radial velocity, and FWHM velocity dispersion (instrument broadening removed) maps in Figure 3. H α is the only emission line that has a signal-to-noise ratio high enough for this purpose. We employ a 2×2 pixel binning for the flux and velocity maps, and a 3×3 binning for the FWHM map to improve the statistics.

We mark three particular regions on the map (see Figure 4). Region 1 is a $2''$ wide elliptical annulus along the edge of the bubble, excluding the eastern end where it overlaps with region 3. This is the outermost region of the bubble, and represents the part with the lowest FWHM. Region 2, i.e., the ULX region, is a $2''$ -radius circle around the X-ray position, which is blue shifted compared with other regions. Region 3 is a low flux cavity in the eastern part of the bubble. The velocity and velocity dispersion measured with H α , [S II], and [O III] in the three regions are listed in Table 2.

3.1. Line decomposition

We suppose that the line kinematics seen on each pixel of the nebula is a result of both approaching and receding motions, with respect to the systematic velocity (also see Soria et al. 2021). Region 1, which is along the edge of the bubble, shows a radial velocity well consistent with the systematic velocity, and a FWHM among the lowest in the bubble, indicating that the gases along the edge may be moving transversally. If this is the case, the FWHM in region 1 reflects the intrinsic line width of the shock, which is around $\sim 70 \text{ km s}^{-1}$ (see Table 2).

Due to the presence of strong low ionization forbidden lines, such as [O I], [S II] and [N II], the shock is believed to be radiative instead of adiabatic (Heng 2010; Soria et al. 2021). For radiative shocks, it is not straightforward to infer the local shock velocity from the gas velocity dispersion (see Appendix A in Soria et al. 2021). Following their recipe, which is based on the assumption of a uniformly expanding

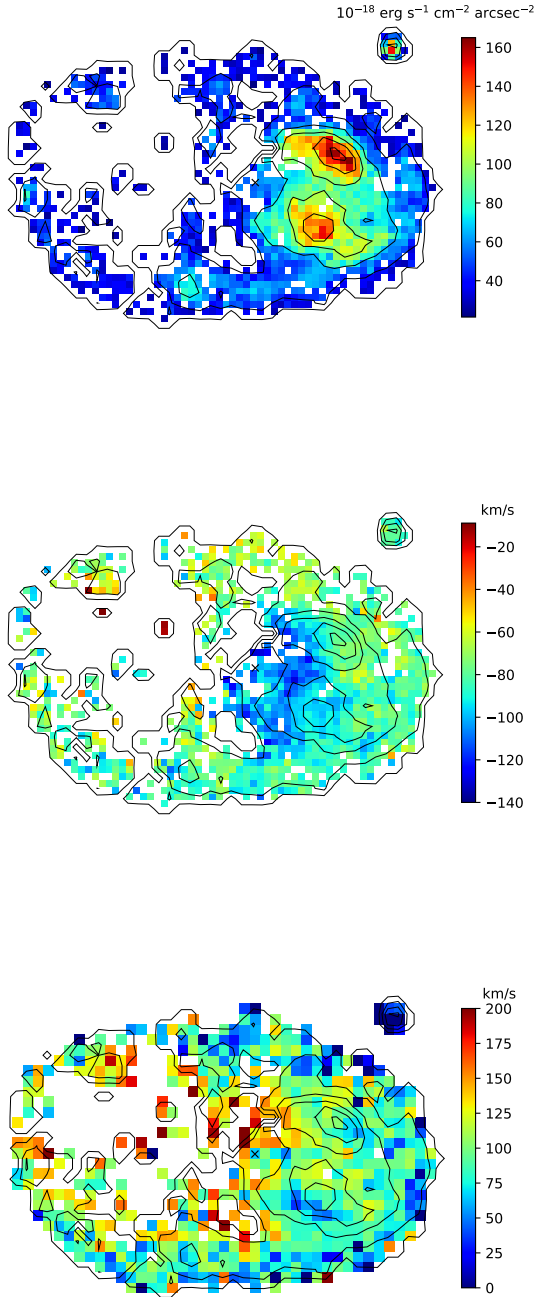


Figure 3. $H\alpha$ flux (**top**), radial velocity (**middle**), and FWHM velocity dispersion (**bottom**) maps of the NGC 1313 X-2 nebula, on top of the flux contours. The former two have a binning of 2×2 original pixels and the last one is binned by 3×3 pixels before spectral fitting. Pixels are not shown if the emission line cannot be determined at a significance of 2σ . The position of the X-ray source is indicated by a cross.

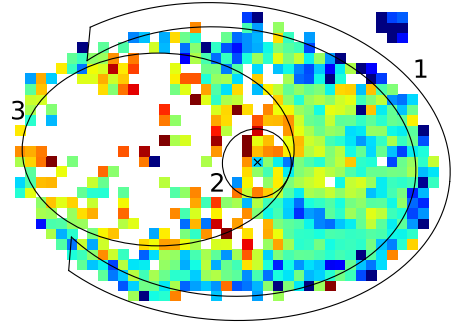


Figure 4. Three regions on the $H\alpha$ FWHM map. Region 1 is a $2''$ wide elliptical annulus referring to the edge of the bubble nebula excluding the part overlapped with region 3. Region 2 is a $2''$ -radius circle centered on the ULX position. Region 3 (with region 2 excluded) indicates a flux cavity.

Table 2. Velocities and velocity dispersions in the three regions defined in Figure 4 for $H\alpha$, [S II], and [O III].

| Region | v (km s^{-1}) | FWHM (km s^{-1}) |
|-------------------------------------|-------------------------------|--------------------------------|
| $H\alpha$ | | |
| 1: edge | -81.0 ± 0.4 | 73 ± 2 |
| 2: ULX | -106.5 ± 1.1 | 136 ± 4 |
| 3: cavity | -76.4 ± 0.9 | 160 ± 3 |
| [S II] $\lambda\lambda 6716, 6731$ | | |
| 1: edge | -76.6 ± 2.1 | 68 ± 10 |
| 2: ULX | -105.9 ± 4.4 | 149 ± 13 |
| 3: cavity | -74.7 ± 3.0 | 158 ± 9 |
| [O III] $\lambda\lambda 4959, 5007$ | | |
| 1: edge | -81.8 ± 6.5 | 76 ± 38 |
| 2: ULX | -107.4 ± 2.8 | 91 ± 14 |
| 3: cavity | -57.2 ± 4.1 | 173 ± 14 |

thin shell, we infer a shock velocity $v_s \approx 0.47\text{FWHM}_2 = 64 \text{ km s}^{-1}$, or $v_s \approx 0.735\text{FWHM}_{\text{all}} = 81 \text{ km s}^{-1}$, where FWHM_2 and FWHM_{all} are the $H\alpha$ FWHM in region 2 (Table 2) and of the whole nebula (Table 1), respectively. Previous studies using long slit spectroscopy argued that the shock

velocity of the nebula could be as high as 80 km s^{-1} (Pakull & Mirioni 2002) or 100 km s^{-1} (Ramsey et al. 2006). Thus, in this study, we assume a shock velocity of 80 km s^{-1} .

Then, we try to model the observed $\text{H}\alpha$ line profile in the ULX region (region 2), where the bulk motion of shocked gas is radial. Here we assume that the shock velocity equals the bulk velocity of shocked gas, which is the observed velocity, in the case of fully radiative shocks (Dopita & Sutherland 2003). We fix the shock velocities to be $\pm 80 \text{ km s}^{-1}$ for the approaching and receding components, respectively, and assume that both have a FWHM of 70 km s^{-1} . The instrument line broadening and measurement noise are taken into account. However, the model line width is significantly larger than the observed line width (Figure 5). We obtain the same conclusions if we fix the FWHM at any value in the range of $50\text{--}100 \text{ km s}^{-1}$.

This may suggest that the emission line has a more complicated velocity distribution (also see the 2D spectrum in Ramsey et al. 2006). Therefore, we add a zero-velocity component with an intrinsic FWHM = 0. The three-component model can fit the line profile adequately, with a flux ratio of 3:3:1 (Figure 5). The 2D spectrum in Ramsey et al. (2006) also shows a hint of a stationary component. The presence of a low-velocity narrow component could be interpreted as due to photoionization.

3.2. Observational evidence for additional photoionization

As mentioned above, the strong [S II] and [O I] emission lines in the nebula are suggestive of predominant shock-ionization (Pakull & Mirioni 2002, 2003). To produce high ionization emission lines like [O III], one requires either high velocity shocks or photoionization.

We display the [O III] $\lambda 5007$ flux map on top of an Hubble Space Telescope (HST) ACS F435W image in Figure 6. As one can see, regions with high [O III] fluxes are spatially coincident with dense stellar populations shown on the HST image. No similar coincidence is seen with the $\text{H}\alpha$ map. This implies that some of the [O III] emission may be attributed to photoionization by massive stars. The [O III] flux in the ULX region (region 2) is also enhanced, possibly caused by additional X-ray irradiation. As one can see in Table 2, the FWHM of [O III] in region 2 is significantly smaller than that of $\text{H}\alpha$ and [S II], implying that the [O III] emission is perhaps due to a different ionizing mechanism.

3.3. Comparison with MAPPINGS V

To check if photoionization is needed in addition to shock-ionization, we perform simulations with MAPPINGS V (Sutherland & Dopita 2017). We assume an ISM density of 1 cm^{-3} , a magnetic field of $3 \mu\text{G}$ (Han 2017); these two parameters are not sensitive to the results. We also assume $Z = 0.5Z_{\odot}$ as suggested by previous studies (Ripamonti et al. 2011; Pintore & Zampieri 2012) and will discuss its influence. The models include dust calculations and allow grain destruction; these two options also have a small impact on our conclusions. The pre-ionization state is calculated in a self-consistent manner, taking into account inter-

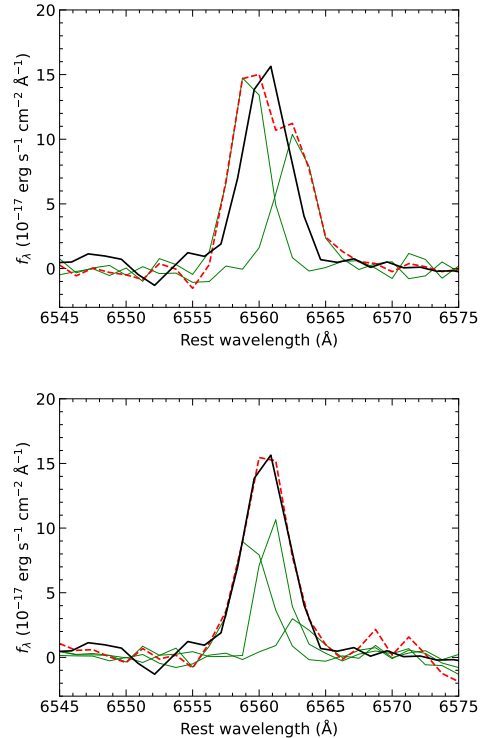


Figure 5. Observed (solid black) and model (dashed red) $\text{H}\alpha$ emission line profiles in region 2. **Top:** the model consists of two components (green), both with a FWHM of 70 km s^{-1} , approaching and receding from the systematic at a velocity of 80 km s^{-1} , respectively. **Bottom:** a third, narrow component at zero-velocity is added

nal photoionization due to post-shock radiation and external photoionization from X-ray sources and O stars.

First, we compare observations with simulations of pure shocks (Model A), and set the shock velocity $v_s = 80 \text{ km s}^{-1}$. However, the simulated [O III] $\lambda 5007$ to $\text{H}\beta$ flux ratio (on the order of 10^{-6}) is significantly lower than that observed (see Table 3). If we set a solar abundance, [O III] $\lambda 5007/\text{H}\beta$ is found to be 0.016, still about two orders of magnitude lower than that observed. To match the observed [O III] $\lambda 5007/\text{H}\beta$, one requires a shock velocity over 100 km s^{-1} at $0.5Z_{\odot}$, or $\approx 85 \text{ km s}^{-1}$ at solar abundance. In these cases, however, the [O I] $\lambda 6300$ to $\text{H}\alpha$ flux ratio is found to be significantly lower than that observed, because most of the oxygens stay at a higher ionization state. To conclude, pure shock-ionization cannot account for both [O III] $\lambda 5007/\text{H}\beta$ and [O I] $\lambda 6300/\text{H}\alpha$.

We thereby add photoionization in addition to shock-ionization (Model B). We add an X-ray source and a certain number of O stars for photoionization illuminating at a distance of 300 pc (length of the semi-major axis of the nebula). The X-ray power-law spectral index is fixed at -1.5 , the typical value found from X-ray fitting (Qiu & Feng 2021). Each

Table 3. Observed and simulated line flux ratios.

| Line flux ratio | Observed | Model A | Model B |
|-------------------------------|---------------------|---------|---------|
| [O III] $\lambda 5007/H\beta$ | 1.269 ± 0.079 | 0.004 | 1.092 |
| [O I] $\lambda 6300/H\alpha$ | 0.171 ± 0.005 | 0.018 | 0.201 |
| $H\alpha/H\beta$ | $2.868 \pm 0.138^*$ | 3.395 | 2.955 |
| [N II] $\lambda 6583/H\alpha$ | 0.154 ± 0.004 | 0.071 | 0.378 |
| [S II] $\lambda 6716/H\alpha$ | 0.400 ± 0.009 | 0.106 | 0.418 |

*The value has been corrected with the Galactic extinction.

NOTE—Model A: pure shock at 80 km s^{-1} . Model B: shock at 80 km s^{-1} with a power-law ($F_\nu \propto \nu^{-1.5}$) X-ray source of $1.6 \times 10^{40} \text{ erg s}^{-1}$ and 60 O stars at 300 pc.

O star has an effective temperature of 40000 K. We vary the X-ray luminosity and O star quantity to fit the observation, and find that an X-ray luminosity of $1.6 \times 10^{40} \text{ erg s}^{-1}$ plus 60 O stars with a total luminosity of $6.4 \times 10^{40} \text{ erg s}^{-1}$ can reasonably match the observations (Table 3). The simulated [N II] $\lambda 6583/H\alpha$ is higher than that observed; this is consistent with previous studies by Ripamonti et al. (2011) who propose that the nitrogen abundance in the nebula could be further lower.

This ULX also displays a soft blackbody component, which could be the ionizing source. We replace the power-law component with a blackbody component and set the temperature at two extremes from observations, 0.1 keV and 0.25 keV (Qiu & Feng 2021). However, it cannot fit the observed flux ratios in the luminosity range of $(0.5 - 50) \times 10^{39} \text{ erg s}^{-1}$. If we further increase the blackbody luminosity to match the observed [O III] $\lambda 5007/H\beta$, the predicted [S II] $\lambda 6716/H\alpha$ is way below that observed.

We also perform a test with a flat ionizing spectrum ($F_\nu \propto \nu^0$) in the EUV to soft X-ray band (40 eV to 1 keV) to mimic emission from a multicolor disk with an innermost temperature of about 0.1 keV. In this case, an X-ray luminosity of $5 \times 10^{40} \text{ erg s}^{-1}$ plus 250 O stars can provide a good fit with the observations except [O I] $\lambda 6300/H\alpha$, which is over-predicted by a factor of 1.6. Thus, we refer to this case as a marginal fit.

The observed $H\alpha$ to $H\beta$ flux ratio is 2.87 ± 0.14 after correction with the Galactic extinction $E(B-V) = 0.075$ along the line of sight (Schlafly & Finkbeiner 2011). This sets the upper bound on the intrinsic $H\alpha/H\beta$. As one can see, the pure shock model (Model A) predicts a higher $H\alpha/H\beta$, inconsistent with the observation, while the model with additional photoionization (Model B) produces an acceptable ratio, if there is no extra reddening in the host galaxy. This is consistent with previous studies (Grisé et al. 2008) that there is no extragalactic extinction for the NGC 1313 X-2 nebula.

In Figure 7, we show the [O III] $\lambda 5007/H\beta$ ratio map on top of the HST F435W image. Regions with enhanced

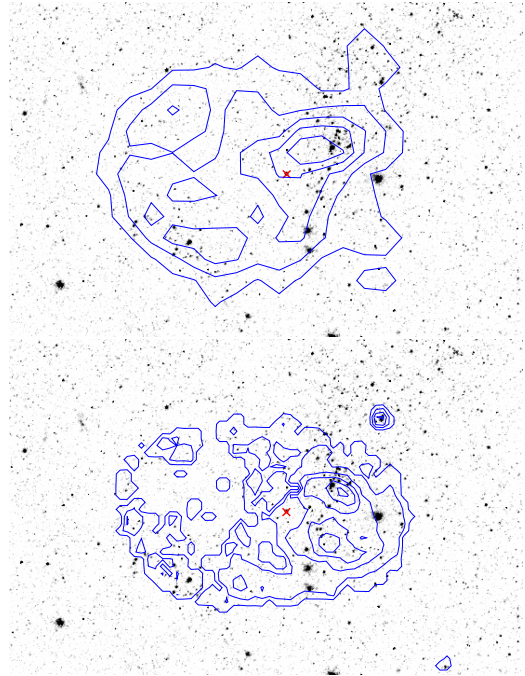
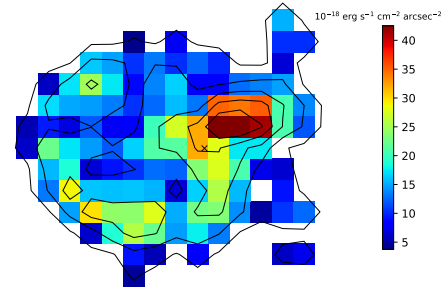


Figure 6. The **top** panel shows the continuum removed [O III] $\lambda 5007$ ($\pm 5 \text{ \AA}$ around the line centroid) flux images around NGC 1313 X-2, with a binning of 9×9 pixels. Those having a signal-to-noise ratio less than 2 are not shown. The **middle** and **bottom** panels display an HST ACS F435W image with [O III] $\lambda 5007$ or $H\alpha$ flux contours, respectively.

[O III] $\lambda 5007/H\beta$ need more contribution from photoionization, including the ULX region and the southeastern and northwestern parts of the nebula. For comparison, the [O I] $\lambda 6300/H\alpha$ map is also shown in Figure 7. The distribution of [O I] $\lambda 6300/H\alpha$ is anti-correlated with that of [O III] $\lambda 5007/H\beta$, as they require oxygens at different ionization states. Particularly, the southwestern region shows high [O I] $\lambda 6300/H\alpha$ and low [O III] $\lambda 5007/H\beta$. We try to model the emission line ratios in this region with Model B, and find that less X-ray luminosity ($7 \times 10^{39} \text{ erg s}^{-1}$) and less number (20) of O stars are needed, compared with that needed for the whole nebula (see Table 3), indicative of a lower pre-ionization state in this region.

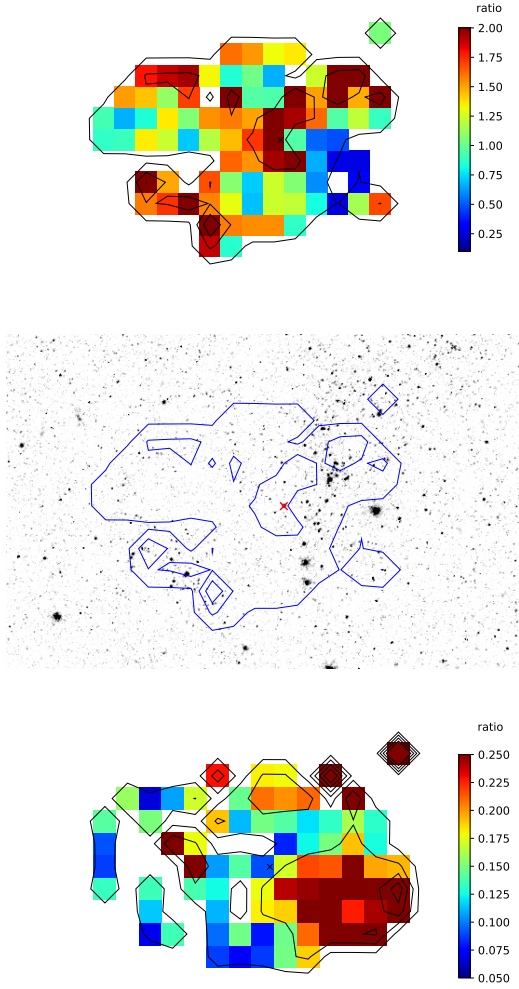


Figure 7. [O III] $\lambda 5007/H\beta$ ratio map (**top**) and its contours on top of the HST F435W image (**middle**). The ratio map has a binning of 9×9 and only shows pixels with a signal-to-noise ratio greater than 2. The cross marks the ULX position. In the **bottom** panel, the [O I] $\lambda 6300/H\alpha$ ratio map is displayed for comparison; it shows an anti-correlation with the [O III] $\lambda 5007/H\beta$ map.

3.4. Total power

Following Pakull & Mirioni (2002), here we estimate the mechanical power of the wind/jet that inflates the bubble. The $H\beta$ surface brightness ($S_{H\beta}$) is a function of the shock velocity (v_s) and the pre-shock ISM number density (n_{ISM} ; Dopita & Sutherland 1996),

$$\frac{S_{H\beta}}{\text{erg s}^{-1} \text{cm}^{-2}} = 7.44 \times 10^{-6} \left(\frac{v_s}{10^2 \text{ km s}^{-1}} \right)^{2.41} \left(\frac{n_{\text{ISM}}}{\text{cm}^3} \right). \quad (1)$$

Observationally, the surface brightness can be calculated via the line luminosity ($L_{H\beta}$) or observed line flux ($f_{H\beta}$),

$$S_{H\beta} = \frac{L_{H\beta}}{4\pi R_B^2} = \frac{f_{H\beta}}{\theta_B^2}, \quad (2)$$

where R_B and θ_B are the physical radius and angular radius, respectively, of the nebula. Here we take the size of the semi-major axis of the nebula into calculation. We take a shock velocity $v_s = 80 \text{ km s}^{-1}$ and assume Galactic extinction only. Thus, for the whole nebula, we obtain an average $n_{\text{ISM}} = (0.45 \pm 0.02) \text{ cm}^{-3}$.

Assuming a pressure driven nebula (Weaver et al. 1977), the wind/jet power (P) and the age of the nebula (t) are related with other properties of the nebula as follows,

$$R_B \approx 0.76 t^{\frac{3}{5}} \left(\frac{P}{\rho_0} \right)^{\frac{1}{5}}, \quad (3)$$

$$v_s \approx 0.38 \left(\frac{P}{R_B^2 \rho_0} \right)^{\frac{1}{3}}, \quad \text{and} \quad (4)$$

$$t = \frac{3R_B}{5v_s}, \quad (5)$$

where $\rho_0 = \mu m_p n_{\text{ISM}}$ is the pre-shock density of the ISM, m_p is the proton mass, and $\mu \approx 1.2$ is the average atomic weight assuming neutral gas with $Z = 0.5Z_\odot$. Plugging in R_B and n_{ISM} and considering the measurement uncertainties, we get

$$t \approx 2.1 \text{ Myr}, \quad (6)$$

and

$$P = (6.5 \pm 0.3) \times 10^{39} \text{ erg s}^{-1}. \quad (7)$$

All these results are generally consistent with those reported previously (e.g., Pakull & Mirioni 2002).

4. DISCUSSION

With the MUSE data, we obtain results consistent with previous studies for the whole nebula. The flux, velocity, velocity dispersion maps help reveal interesting structures inside the bubble. The surface brightness is scaled with shock velocity and ISM density. Therefore, the low surface brightness in region 3 can be explained as a result of a low ISM density.

In region 2 (ULX region), where the gas bulk motion is radial, we find that a simple two-component (approaching and receding) model cannot fit the line profile, and a third low-velocity narrow component is needed. Such a component could be a hint of photoionization. We find spatial correlation between the [O III] emission and clusters of stars, as well as enhanced [O III] emission in region 2 around the ULX, suggesting that some of the [O III] emission may be due to photoionization. Simulations with *MAPPINGS V* also suggest that pure shocks are unable to account for the observed line ratios; shocks with $\leq 80 \text{ km s}^{-1}$ cannot produce [O III] $\lambda 5007/H\beta$ as high as that observed, while shocks with higher velocities that are able to reproduce the observed [O III] $\lambda 5007/H\beta$ cannot explain the observed high

value of [O I]/H α due to over-ionization. Adding photoionization to shocks of 80 km s⁻¹ can reproduce the observations. In that case, the X-ray luminosity is derived to be close to 10⁴⁰ erg s⁻¹, which is comparable to but slightly higher than the typical isotropic luminosity (several times 10³⁹ erg s⁻¹) of NGC 1313 X-2 inferred from X-ray observations (Qiu & Feng 2021). We note that both luminosities are derived assuming an illuminating distance of 300 pc. If the emission line clouds are located at a smaller distance to the source, a lower luminosity is required. For X-rays, a reduced distance by a factor less than 2 can match the luminosity seen from X-ray observations. For O stars, as the brightest [O III] region is spatially coincident with star clusters, they could be close in distance and only a few of them can account for the needed luminosity (e.g., one or two O stars at a distance of 50 pc). Therefore, the presence of these ionizing sources can account for the power needed for photoionization. However, the power-law component extrapolated from the X-ray band may cut off at energies above EUV, while the blackbody component observed in the soft X-ray band cannot provide sufficient ionization. Alternatively, a flat ionizing spectrum with a higher X-ray luminosity (5×10^{40} erg s⁻¹) plus more O stars

(~ 250), both at 300 pc, can provide a marginal fit. If this is the case, it may suggest that the X-ray ionizing source is a multicolor accretion flow and the ionizing distance is smaller than that assumed, e.g., 1.4×10^{39} erg s⁻¹ at 50 pc. We note that, although the total luminosity seems to fit the observation, one should keep in mind that the origin of the X-ray source for ionization is still uncertain.

Additional photoionization may affect the the estimation of the wind/jet power that is based on a shock model (Weaver et al. 1977). However, the current data do not allow us to accurately quantify the luminosity and spectrum of the photoionization source. Also, the extra photoionization changes the pre-ionization state and has a nonlinear contribution to the production of emission lines. Therefore, we may treat the inferred power as an upper limit of the wind/jet power for the ULX.

We thank the anonymous referee for useful comments. HF acknowledges funding support from the National Key R&D Project under grant 2018YFA0404502, the National Natural Science Foundation of China under grants Nos. 12025301 & 11821303, and the Tsinghua University Initiative Scientific Research Program.

REFERENCES

- Abarca, D., Kluźniak, W., & Sądowski, A. 2018, *MNRAS*, 479, 3936, doi: [10.1093/mnras/sty1602](https://doi.org/10.1093/mnras/sty1602)
- Abolmasov, P. 2008, in *American Institute of Physics Conference Series*, Vol. 1054, *Cool Discs, Hot Flows: The Varying Faces of Accreting Compact Objects*, ed. M. Axelsson, 33–38, doi: [10.1063/1.3002506](https://doi.org/10.1063/1.3002506)
- Abolmasov, P., Fabrika, S., Sholukhova, O., & Afanasiev, V. 2007, *Astrophysical Bulletin*, 62, 36, doi: [10.1134/S199034130701004X](https://doi.org/10.1134/S199034130701004X)
- Bachetti, M., Harrison, F. A., Walton, D. J., et al. 2014, *Nature*, 514, 202, doi: [10.1038/nature13791](https://doi.org/10.1038/nature13791)
- Bacon, R., Accardo, M., Adjali, L., et al. 2010, in *Society of Photo-Optical Instrumentation Engineers (SPIE) Conference Series*, Vol. 7735, *Ground-based and Airborne Instrumentation for Astronomy III*, ed. I. S. McLean, S. K. Ramsay, & H. Takami, 773508, doi: [10.1117/12.856027](https://doi.org/10.1117/12.856027)
- Belfiore, A., Esposito, P., Pintore, F., et al. 2020, *Nature Astronomy*, 4, 147, doi: [10.1038/s41550-019-0903-z](https://doi.org/10.1038/s41550-019-0903-z)
- Carpano, S., Haberl, F., Maitra, C., & Vasilopoulos, G. 2018, *MNRAS*, 476, L45, doi: [10.1093/mnrasl/sly030](https://doi.org/10.1093/mnrasl/sly030)
- Colbert, E. J. M., Petre, R., Schlegel, E. M., & Ryder, S. D. 1995, *ApJ*, 446, 177, doi: [10.1086/175777](https://doi.org/10.1086/175777)
- Dopita, M. A., & Sutherland, R. S. 1996, *ApJS*, 102, 161, doi: [10.1086/192255](https://doi.org/10.1086/192255)
- . 2003, *Astrophysics of the diffuse universe* (Berlin: Springer)
- Fürst, F., Walton, D. J., Harrison, F. A., et al. 2016, *ApJL*, 831, L14, doi: [10.3847/2041-8205/831/2/L14](https://doi.org/10.3847/2041-8205/831/2/L14)
- Gaia Collaboration, Brown, A. G. A., Vallenari, A., et al. 2021, *A&A*, 649, A1, doi: [10.1051/0004-6361/202039657](https://doi.org/10.1051/0004-6361/202039657)
- Grisé, F., Pakull, M. W., Soria, R., et al. 2008, *A&A*, 486, 151, doi: [10.1051/0004-6361:200809557](https://doi.org/10.1051/0004-6361:200809557)
- Han, J. L. 2017, *ARA&A*, 55, 111, doi: [10.1146/annurev-astro-091916-055221](https://doi.org/10.1146/annurev-astro-091916-055221)
- Hashizume, K., Ohsuga, K., Kawashima, T., & Tanaka, M. 2015, *PASJ*, 67, 58, doi: [10.1093/pasj/psu132](https://doi.org/10.1093/pasj/psu132)
- Heng, K. 2010, *PASA*, 27, 23, doi: [10.1071/AS09057](https://doi.org/10.1071/AS09057)
- Israel, G. L., Belfiore, A., Stella, L., et al. 2017a, *Science*, 355, 817, doi: [10.1126/science.aai8635](https://doi.org/10.1126/science.aai8635)
- Israel, G. L., Papitto, A., Esposito, P., et al. 2017b, *MNRAS*, 466, L48, doi: [10.1093/mnrasl/slw218](https://doi.org/10.1093/mnrasl/slw218)
- Jiang, Y.-F., Stone, J. M., & Davis, S. W. 2014, *ApJ*, 796, 106, doi: [10.1088/0004-637X/796/2/106](https://doi.org/10.1088/0004-637X/796/2/106)
- Kaaret, P., Feng, H., & Roberts, T. P. 2017, *ARA&A*, 55, 303, doi: [10.1146/annurev-astro-091916-055259](https://doi.org/10.1146/annurev-astro-091916-055259)
- King, A. R., & Pounds, K. A. 2003, *MNRAS*, 345, 657, doi: [10.1046/j.1365-8711.2003.06980.x](https://doi.org/10.1046/j.1365-8711.2003.06980.x)
- Kitaki, T., Mineshige, S., Ohsuga, K., & Kawashima, T. 2018, *PASJ*, 70, 108, doi: [10.1093/pasj/psy110](https://doi.org/10.1093/pasj/psy110)
- . 2021, *PASJ*, 73, 450, doi: [10.1093/pasj/psab011](https://doi.org/10.1093/pasj/psab011)
- Koribalski, B. S., Staveley-Smith, L., Kilborn, V. A., et al. 2004, *AJ*, 128, 16, doi: [10.1086/421744](https://doi.org/10.1086/421744)

- Kosec, P., Pinto, C., Walton, D. J., et al. 2018, *MNRAS*, 479, 3978, doi: [10.1093/mnras/sty1626](https://doi.org/10.1093/mnras/sty1626)
- Lipunova, G. V. 1999, *Astronomy Letters*, 25, 508. <https://arxiv.org/abs/astro-ph/9906324>
- Liu, J.-F., Bregman, J., Miller, J., & Kaaret, P. 2007, *ApJ*, 661, 165, doi: [10.1086/516624](https://doi.org/10.1086/516624)
- Meier, D. L. 1982, *ApJ*, 256, 681, doi: [10.1086/159942](https://doi.org/10.1086/159942)
- Mineo, S., Gilfanov, M., & Sunyaev, R. 2012, *MNRAS*, 419, 2095, doi: [10.1111/j.1365-2966.2011.19862.x](https://doi.org/10.1111/j.1365-2966.2011.19862.x)
- Mucciarelli, P., Zampieri, L., Falomo, R., Turolla, R., & Treves, A. 2005, *ApJL*, 633, L101, doi: [10.1086/498448](https://doi.org/10.1086/498448)
- Ohsuga, K., & Mineshige, S. 2011, *ApJ*, 736, 2, doi: [10.1088/0004-637X/736/1/2](https://doi.org/10.1088/0004-637X/736/1/2)
- Pakull, M. W., & Grisé, F. 2008, in *American Institute of Physics Conference Series*, Vol. 1010, *A Population Explosion: The Nature & Evolution of X-ray Binaries in Diverse Environments*, ed. R. M. Bandyopadhyay, S. Wachter, D. Gelino, & C. R. Gelino, 303–307, doi: [10.1063/1.2945062](https://doi.org/10.1063/1.2945062)
- Pakull, M. W., Grisé, F., & Motch, C. 2006, in *Populations of High Energy Sources in Galaxies*, ed. E. J. A. Meurs & G. Fabbiano, Vol. 230, 293–297, doi: [10.1017/S1743921306008489](https://doi.org/10.1017/S1743921306008489)
- Pakull, M. W., & Mirioni, L. 2002, *arXiv e-prints*, astro. <https://arxiv.org/abs/astro-ph/0202488>
- Pakull, M. W., & Mirioni, L. 2003, in *Revista Mexicana de Astronomia y Astrofisica Conference Series*, Vol. 15, *Revista Mexicana de Astronomia y Astrofisica Conference Series*, ed. J. Arthur & W. J. Henney, 197–199
- Pinto, C., Middleton, M. J., & Fabian, A. C. 2016, *Nature*, 533, 64, doi: [10.1038/nature17417](https://doi.org/10.1038/nature17417)
- Pinto, C., Alston, W., Soria, R., et al. 2017, *MNRAS*, 468, 2865, doi: [10.1093/mnras/stx641](https://doi.org/10.1093/mnras/stx641)
- Pinto, C., Soria, R., Walton, D. J., et al. 2021, *MNRAS*, 505, 5058, doi: [10.1093/mnras/stab1648](https://doi.org/10.1093/mnras/stab1648)
- Pintore, F., & Zampieri, L. 2012, *MNRAS*, 420, 1107, doi: [10.1111/j.1365-2966.2011.20072.x](https://doi.org/10.1111/j.1365-2966.2011.20072.x)
- Pintore, F., Zampieri, L., Stella, L., et al. 2017, *ApJ*, 836, 113, doi: [10.3847/1538-4357/836/1/113](https://doi.org/10.3847/1538-4357/836/1/113)
- Poutanen, J., Lipunova, G., Fabrika, S., Butkevich, A. G., & Abolmasov, P. 2007, *MNRAS*, 377, 1187, doi: [10.1111/j.1365-2966.2007.11668.x](https://doi.org/10.1111/j.1365-2966.2007.11668.x)
- Qing, G., Wang, W., Liu, J.-F., & Yoachim, P. 2015, *ApJ*, 799, 19, doi: [10.1088/0004-637X/799/1/19](https://doi.org/10.1088/0004-637X/799/1/19)
- Qiu, Y., & Feng, H. 2021, *ApJ*, 906, 36, doi: [10.3847/1538-4357/abc959](https://doi.org/10.3847/1538-4357/abc959)
- Ramsey, C. J., Williams, R. M., Gruendl, R. A., et al. 2006, *ApJ*, 641, 241, doi: [10.1086/499070](https://doi.org/10.1086/499070)
- Ripamonti, E., Mapelli, M., Zampieri, L., & Colpi, M. 2011, *Astronomische Nachrichten*, 332, 418, doi: [10.1002/asna.201011512](https://doi.org/10.1002/asna.201011512)
- Rodríguez Castillo, G. A., Israel, G. L., Belfiore, A., et al. 2020, *ApJ*, 895, 60, doi: [10.3847/1538-4357/ab8a44](https://doi.org/10.3847/1538-4357/ab8a44)
- Russell, D. M., Yang, Y. J., Gladstone, J. C., Wiersema, K., & Roberts, T. P. 2011, *Astronomische Nachrichten*, 332, 371, doi: [10.1002/asna.201011502](https://doi.org/10.1002/asna.201011502)
- Sathyaprakash, B., Bailes, M., Kasliwal, M. M., et al. 2019, *BAAS*, 51, 276. <https://arxiv.org/abs/1903.09277>
- Sądowski, A., & Narayan, R. 2016, *MNRAS*, 456, 3929, doi: [10.1093/mnras/stv2941](https://doi.org/10.1093/mnras/stv2941)
- Schlafly, E. F., & Finkbeiner, D. P. 2011, *ApJ*, 737, 103, doi: [10.1088/0004-637X/737/2/103](https://doi.org/10.1088/0004-637X/737/2/103)
- Shakura, N. I., & Sunyaev, R. A. 1973, *A&A*, 24, 337
- Shen, R.-F., Nakar, E., & Piran, T. 2016, *MNRAS*, 459, 171, doi: [10.1093/mnras/stw645](https://doi.org/10.1093/mnras/stw645)
- Soria, R., Pakull, M. W., Motch, C., et al. 2021, *MNRAS*, 501, 1644, doi: [10.1093/mnras/staa3784](https://doi.org/10.1093/mnras/staa3784)
- Storey, P. J., & Zeppen, C. J. 2000, *MNRAS*, 312, 813, doi: [10.1046/j.1365-8711.2000.03184.x](https://doi.org/10.1046/j.1365-8711.2000.03184.x)
- Sutherland, R. S., & Dopita, M. A. 2017, *ApJS*, 229, 34, doi: [10.3847/1538-4365/aa6541](https://doi.org/10.3847/1538-4365/aa6541)
- Takahashi, H. R., Ohsuga, K., Kawashima, T., & Sekiguchi, Y. 2016, *ApJ*, 826, 23, doi: [10.3847/0004-637X/826/1/23](https://doi.org/10.3847/0004-637X/826/1/23)
- Walton, D. J., Middleton, M. J., Pinto, C., et al. 2016, *ApJL*, 826, L26, doi: [10.3847/2041-8205/826/2/L26](https://doi.org/10.3847/2041-8205/826/2/L26)
- Walton, D. J., Fürst, F., Heida, M., et al. 2018, *ApJ*, 856, 128, doi: [10.3847/1538-4357/aab610](https://doi.org/10.3847/1538-4357/aab610)
- Weaver, R., McCray, R., Castor, J., Shapiro, P., & Moore, R. 1977, *ApJ*, 218, 377, doi: [10.1086/155692](https://doi.org/10.1086/155692)
- Weilbacher, P. M., Palsa, R., Streicher, O., et al. 2020, *A&A*, 641, A28, doi: [10.1051/0004-6361/202037855](https://doi.org/10.1051/0004-6361/202037855)
- Zampieri, L., Mucciarelli, P., Falomo, R., et al. 2004, *ApJ*, 603, 523, doi: [10.1086/381541](https://doi.org/10.1086/381541)